UC Irvine
UC Irvine Previously Published Works

Title

Ground-state phase diagram of the t-t′-J model

Permalink

https://escholarship.org/uc/item/8tj188zs

Journal

Proceedings of the National Academy of Sciences of the United States of America, 118(44)

ISSN

0027-8424

Authors

Jiang, Shengtao
Scalapino, Douglas J
White, Steven R

Publication Date

2021-11-02

DOI

10.1073/pnas.2109978118

Peer reviewed

Ground-state phase diagram of the *t-t'-J* model

Shengtao Jiang[a], Douglas J. Scalapino[b], and Steven R. White[a,1]

[a]Department of Physics and Astronomy, University of California, Irvine, CA 92697; and [b]Department of Physics, University of California, Santa Barbara, CA 93106

We report results of large-scale ground-state density matrix renormalization group (DMRG) calculations on t-t'-J cylinders with circumferences 6 and 8. We determine a rough phase diagram that appears to approximate the two-dimensional (2D) system. While for many properties, positive and negative t' values ($t'/t = \pm 0.2$) appear to correspond to electron- and hole-doped cuprate systems, respectively, the behavior of superconductivity itself shows an inconsistency between the model and the materials. The $t' < 0$ (hole-doped) region shows antiferromagnetism limited to very low doping, stripes more generally, and the familiar Fermi surface of the hole-doped cuprates. However, we find $t' < 0$ strongly suppresses superconductivity. The $t' > 0$ (electron-doped) region shows the expected circular Fermi pocket of holes around the (π, π) point and a broad low-doped region of coexisting antiferromagnetism and d-wave pairing with a triplet p component at wavevector (π, π) induced by the antiferromagnetism and d-wave pairing. The pairing for the electron low-doped system with $t' > 0$ is strong and unambiguous in the DMRG simulations. At larger doping another broad region with stripes in addition to weaker d-wave pairing and striped p-wave pairing appears. In a small doping region near $x = 0.08$ for $t' \sim -0.2$, we find an unconventional type of stripe involving unpaired holes located predominantly on chains spaced three lattice spacings apart. The undoped two-leg ladder regions in between mimic the short-ranged spin correlations seen in two-leg Heisenberg ladders.

superconductivity | DMRG | cuprate

There has been considerable recent progress in numerical simulations of the models associated with the cuprate superconductors—the two-dimensional (2D) Hubbard and t-J models and their variants (1–21). Like the materials themselves, these models have been found to exhibit a rich variety of phenomena, ranging from uniform antiferromagnetism (AFM) and d-wave superconductivity (SC) to charge and spin stripes. Some previously controversial issues have been mostly resolved, such as the existence of stripes. Striped states were first found as a Hartree–Fock solution to the doped Hubbard model (22–25), and in the late 1990s two of us used the density matrix renormalization group (26, 27) and found stripes as the ground state of the t-J model (28). At that time this result was controversial, since other powerful simulation methods, such as variational Monte Carlo, could not confirm our results (29, 30). In the last few years, with progress in a variety of methods combined with the use of several simulation methods together, striped ground states have been confirmed not just in the t-J model (8, 13, 14, 31), but also in the Hubbard model (1, 5–7, 11, 15, 32). While d-wave singlet pairing has consistently been favored over other types of pairing in many approaches, it has been less clear in both the t-J and Hubbard models whether the ground state is superconducting or not. The role of stripes in competing against or enhancing pairing has also been difficult to determine. It has long been clear, however, that next nearest-neighbor hopping t' has a crucial influence on the pairing. With a $-t_{ij}$ sign convention for hopping, our early density matrix renormalization group (DMRG) for the t-J model found that a positive t' stabilizes the com-

mensurate (π, π) antiferromagnetic correlations and enhances the d-wave pairing correlations, whereas a negative t' seemed to disfavor these correlations (16, 33). Other work has suggested instead that a negative t' is important in destabilizing stripes so that SC can occur (5).

While DMRG has not changed fundamentally since the 1990s, there have been steady improvements in techniques, software, and computers since then. Here we have used these developments to return to a study of the t-t'-J model. We report here a detailed description of the ground-state phase diagram as a function of t' and doping x, based on $L \times 8$ cylinders with L up to 50, with confirmation of the qualitative features using width-6 cylinders. Note that this model can be used to describe both the hole- and electron-doped cuprates: For $t'/t < 0$ it describes a hole-doped system with electron filling $n_e = 1 - x$, while for $t'/t > 0$, based on a particle–hole transformation, it describes an electron-doped system with $n_e = 1 + x$.

Two important results of our study are 1) the finding of a coexistent antiferromagnetic d-wave SC and induced π-triplet p-wave SC regime in the electron-doped system and 2) the lack of long-range SC order in the hole-doped case.

This paper is organized as follows: In *Model and Method* we introduce the t-t'-J model, the DMRG methods used, and the main observables that we study. In *Phase Diagram* we show the $t' - x$ ground-state phase diagram for $J/t = 0.4$ obtained from the $8 \times L$ cylinder calculations. Here the spin, charge, and d-wave pairing strength for $t'/t = \pm 0.2$ are shown as the

doping x varies slowly along the length of the cylinder. Combined with similar calculations with doping x fixed and t' slowly varying along the length of the cylinder, these results (details shown in *Scans Varying Doping and* t') are used to determine the $t' - x$ ground-state phase diagram.

The resulting phase diagram exhibits four distinct regions. In *Electron Low-Doped Phase with Coexisting Uniform AFM, d-Wave Singlet, and* (π,π) *p-Wave Triplet Pairing* we examine the lightly ($x \lesssim 0.14$) electron-doped region in which there is coexisting AFM and strong d-wave pairing order. In addition there is necessarily also a p-wave triplet pairing component with center of mass momentum (π, π). This order parameter does not depend upon a p-wave pairing interaction, but is dynamically generated by coexisting AFM and d-wave SC order parameters (34–38). While it has the same form as the generator of infinitesimal rotations between AFM and SC order parameters in the $SO(5)$ theory (35), it appears here as an additional order parameter. Its strength relative to the AFM and d-wave order are discussed. In the more heavily doped electron region discussed in *Higher Electron-Doping Phase: Stripes with d-Wave Singlet and Striped p-Wave Pairing* we find stripes with local AFM and weaker d-wave and p-wave triplet pairing. In *Conventional Stripe Phase and Low-Doped W3 Stripe Phase* we discuss the $t' < 0$ part of the phase diagram where we find conventional stripes and an unconventional width-3 stripe phase (W3 stripe) region but negligible pairing. In *Energy Gaps* we study the single particle gap as well as the pair gap for the different phases. In *Comparison to Cuprates* we discuss the relationship of the sign of t' to the electron- and hole-doped cuprates and compare our results to experiments. *Summary* contains our conclusions.

Model and Method

We study the t-t'-J model on a square lattice, with Hamiltonian

$$H = \sum_{\langle ij \rangle \sigma} -t(c_{i\sigma}^{\dagger} c_{j\sigma} + h.c.) + \sum_{\langle\langle ij \rangle\rangle \sigma} -t'(c_{i\sigma}^{\dagger} c_{j\sigma} + h.c.)$$

$$+ J \sum_{\langle ij \rangle} \left(\vec{S}_i \cdot \vec{S}_j - \frac{1}{4} n_i^{tot} n_j^{tot} \right) - \mu \sum_i n_i^{tot}. \qquad \textbf{[1]}$$

Here $n_i^{tot} = n_{i\uparrow} + n_{i\downarrow}$ is the total particle density on site i. $\langle ij \rangle$ denotes nearest-neighbor pairs of sites and $\langle\langle ij \rangle\rangle$ denotes next nearest-neighbor pairs of sites. Doubly occupied states are specifically excluded in the Hilbert space. For all calculations we set $t = 1$ and $J = 0.4$. A chemical potential μ is used to control the doping level in some of the calculations; in others the number of particles is fixed. We study cylinders, with open boundary conditions in the x direction and periodic boundary conditions in the y direction. We study width-6 and width-8 cylinders with lengths up to 50. Our primary focus is on the width-8 systems. Behavior in width 6 is similar and provides an indication that our width-8 results are relevant for 2D.

We use finite-system DMRG using the ITensor library (39). For this size system, keeping about 3,000 to 4,000 states is sufficient to measure local properties, provided that the calculation is not stuck in a metastable state. To control this issue, we perform a variety of simulations with different starting states and temporary pinning fields, comparing energies and convergence of different states, to gain an understanding of the low-energy states and their orders. Some of the details of this process in subtle cases are discussed below. In many cases, such as a conventional striped state, starting in a product state with the holes near where they end up is all that is necessary, but one should try different fillings and spacings of the stripes. For example, eight holes in a striped state might make either two four-hole stripes or four two-hole stripes. In such a case we would try both possibilities and compare energies.

We focus on local measurements of the density, the magnetization, and pairing. The hole density and magnetization are measured using $S_z = \frac{1}{2}(n_{i\uparrow} - n_{i\downarrow})$ and $n_{hole} = 1 - n_{i\uparrow} - n_{i\downarrow}$. To detect the superconducting order and structure in the grand canonical ensemble, we use the singlet (s) and triplet (t) link pairing operators

$$\Delta_{s,t}^{\dagger}(l) = \frac{1}{\sqrt{2}}(c_{l_1,\uparrow}^{\dagger} c_{l_2,\downarrow}^{\dagger} \pm c_{l_2,\uparrow}^{\dagger} c_{l_1,\downarrow}^{\dagger}), \qquad \textbf{[2]}$$

where the $+$ and $-$ are for singlet and triplet, respectively, and l_1 and l_2 are the two sites of link l.

The expectation value $\langle \Delta^{\dagger} + \Delta \rangle$ gives the local pairing strength. For a d-wave superconductor, $\langle \Delta_s^{\dagger} + \Delta_s \rangle$ switches sign between bonds in the x and y directions (40).

Phase Diagram

We begin by presenting the approximate phase diagram of the model in the doping (x)–next-nearest neighbor hopping (t') plane, the detailed features of which are explained later. A key distinction is the difference between positive and negative t'. The t-J model cannot be doped above half-filling, so it does not appear that one can simulate electron-doped cuprates. However, a particle–hole transformation of the single-band Hubbard model maps electron doping to hole doping, but with a change in the sign of t'. One can then view the t-J model as a low-energy description of this particle–hole-transformed Hubbard model. We discuss this in more detail in *Comparison to Cuprates*. The key point is that we can view $t' \approx -0.2$ as applicable to the hole-doped cuprates, while $t' \approx 0.2$ is applicable to the electron-doped cuprates. We refer to the regions of the phase diagram using this terminology.

Our most useful tool in determining the phase diagrams is scan calculations, where in a long cylinder we slowly vary one parameter of the model, either t' or the chemical potential μ, to scan a whole line of the phase diagram. These lines are shown in gray in Fig. 1. These scans are detailed in the next section. Much of the phase diagram is taken up by a phase with conventional stripes. These stripes are lines of increased hole density two or three sites
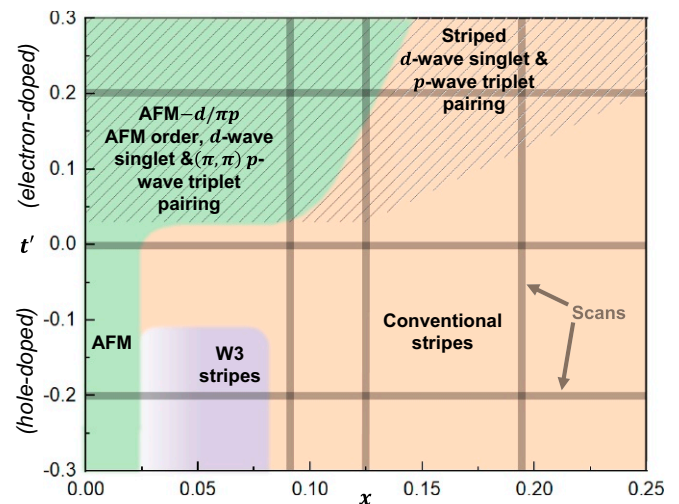
Fig. 1. Approximate phase diagram in the $x - t'$ plane, where x is the doping and t' is the next-nearest neighboring hopping, for width-8 cylinders. The six gray lines indicate the location of parameter-varying "scan" calculations on long cylinders, which were the main tool to determine the phase diagram. Green indicates commensurate AFM order; beige represents conventional stripes, which modulate π-phase shifted domain walls in the AFM order. The slanted lines indicate d-wave pairing order. The simultaneous presence of d-wave pairing and AFM correlations induces weaker momentum-(π, π) p-wave order.

wide, which act as domain walls to π-phase shifted AFM (or at least significant local AFM correlations). Although the holes in these stripes correlate into pairs, the pairs tend to lack phase coherence, and pairing correlations are weak. Significantly, negative t' is found to decrease the pairing correlations. This phase makes up most of the $t' < 0$ side of the diagram.

There is also a type of unconventional striped phase in a small region of the phase diagram with $t' < 0$. In this W3 striped phase, the stripes are predominately one site wide with exactly two rows of mostly undoped sites between them acting as a spin ladder. The holes within stripes are unpaired with a spacing of about 4 between holes. The Heisenberg two-leg ladder is spin gapped, with very short-range spin correlations (41), and the "ladders" in the W3 phase behave similarly. The stripes in W3 do not induce a π-phase shift to the spins on either side, probably due to the combination of low doping within the stripe and the short-range spin correlations. Instead of acting as domain walls, they decouple the spin ladders. The W3 phase appears to have substantial decoupling between the undoped ladders and the doped chains, and the transverse period is locked at three lattice spacings. The W3 phase (like a t-J chain) (42) does not exhibit pairing. For $t' < 0$, commensurate AFM order is present only very close to zero doping; stripes break up the AFM order very quickly on doping.

For t' positive above a small threshold, one enters a very different low-doped phase. This phase has three types of order simultaneously. The two dominant forms of order are AFM and d-wave superconductivity, which have also been found in recent studies of the Hubbard model with positive t' (17). There are no signs of stripes at low doping, and the magnetic order is commensurate at $Q = (\pi, \pi)$. The d-wave order is robust; unlike in previous studies at $t' = 0$ where determining whether the system is superconducting or not requires careful scaling, here its presence is very clear. These two dominant orders, d-wave pairing and AFM, combine to form a weaker triplet p-wave order

at wavevector $Q = (\pi, \pi)$ (34, 43–48). This order comes about because the AFM order breaks SU(2) symmetry, so that singlet and triplet pairings are no longer distinct, and the nonzero wavevector reflects the wavevector of the AFM order. There is no separate attractive conventional interaction in the p channel; this derivative order is purely a consequence of the other two orders.

In the higher-doped $t' > 0$ region, a superconducting striped phase appears. This phase looks locally much like the lower-doped phase, but with stripes. The stripes look like conventional stripes in most respects, but they exhibit significant d-wave pairing, unlike the $t' < 0$ striped phase. The stripes act as domain walls to the AFM order, and locally one sees derivative πp triplet order as well, modulated by the stripes. The pairing overall is somewhat weaker in the higher-doped phase, probably because of the stripes. However, although the stripes somewhat compete with superconductivity, the main driver against pairing appears to be negative t' itself, rather than t' acting through stripe formation. A likely mechanism for this is that positive t' directly increases the mobility of pairs (49), making it easy for them to phase cohere and to avoid becoming locked into stripes.

In Fig. 2 we show nonscan simulations of three of the phases, emphasizing their differences. An alternate view is given by the high-probability product state plots shown in Fig. 2 B, D, and F. These product states are determined from the ground state by a limited search for the most probable product state. One way to search for a probable spin configuration is to sequentially go through the sites of the lattice and, at each site, pick the most probable spin state. After each spin is picked, the wavefunction is projected to reflect this, just as a physical measurement of spin i (say finding the up state) would leave the wavefunction projected into the associated up-i space. However, this approach fails in the presence of holes, since at low doping there are far fewer holes than spins, and the holes end up appearing at the end of the search path, i.e., mostly on the right side of the
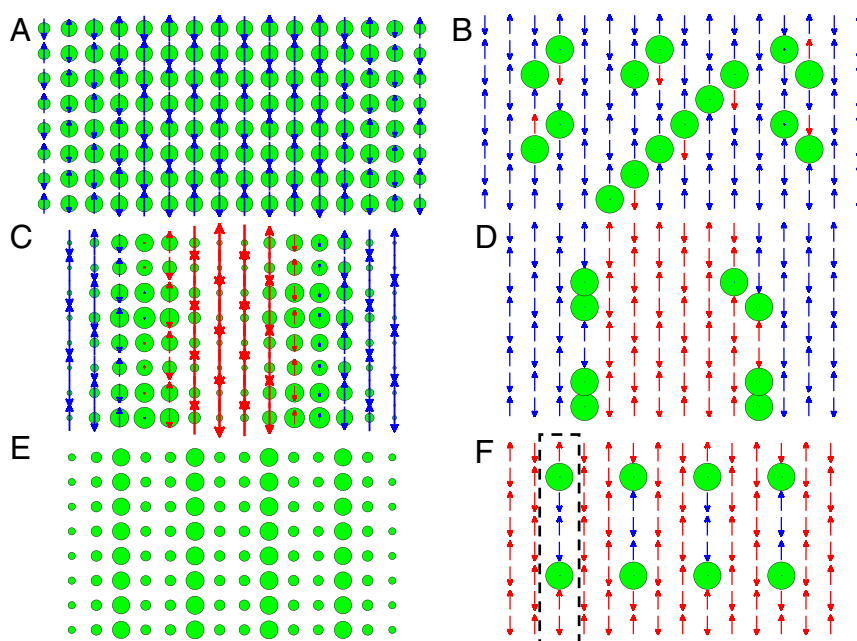

Fig. 2. Local properties (A, C, and E) and a high-probability product state (B, D, and F) of systems in different phases. A, C, and E show conventional local measurements for ground states in three different phases. The length of the arrows and the area of the circles represent $\langle S_z \rangle$ and local doping, respectively. The spins are colored to indicate different AFM domains. B, D, and F show particular product states that occurred with maximum probability in a particular search within the corresponding state (see text). (A and B) Electron low-doped phase with $t' = 0.2$, $x = 0.12$, with simultaneous pairing and AFM order. The highest-probability configuration of a pair of holes is diagonal next-nearest neighbor. (C and D) Conventional stripe phase at $t' = 0$, $x = 0.07$, where half-filled stripes form, and pairing is visible within the stripes, but lacking phase coherence. (E and F) W3 striped phase at $t' = -0.2$, $x = 0.07$, with holes unpaired within the stripes.

Jiang et al.
Ground-state phase diagram of the t-t'-J model

PNAS | 3 of 11
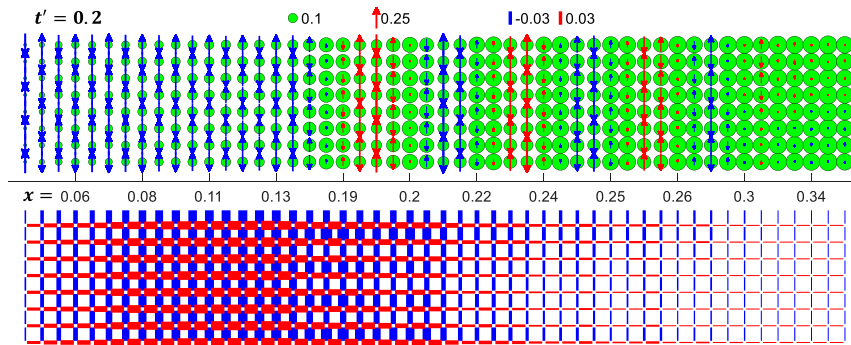https://doi.org/10.1073/pnas.2109978118

Fig. 3. A doping-varying scan on a 50 × 8 cylinder with $t' = 0.2$, appropriate for electron-doped cuprates. Spin and charge are shown in *Upper* plot in the same way as in Fig. 2. *Lower* plot shows the *d*-wave singlet pairing with its sign/amplitude indicated by the color/thickness of bonds. The numbers on the middle axis indicate the approximate local doping. No pairfield is applied. In the underdoped region ($x \lesssim 0.13$) the system exhibits AFM with strong *d*-wave pairing. In the overdoped region ($x > 0.13$) stripes are present, with pairing persisting to about $x \approx 0.25$ to 0.3.

system, which is a low-probability configuration. Instead, here we search for the hole positions separately, finding the most probable position for a hole over all sites at each step, using the hole density of the projected wavefunction. After the holes are found, then we perform a determination of the spin configuration with a fixed path through the rest of the sites, optimizing each spin and projecting.

This gives a view of the states that is hard to see in local measurements or correlation functions. In particular, in the *d*-wave phase in Fig. 2 *A* and *B*, one sees the holes grouped in pairs, with the most probable configuration of a pair being diagonally next-nearest neighbor, as found in earlier work (50). In Fig. 2*B* one sees an apparent diagonal stripe, but there is no sign of this in the ordinary measurements of Fig. 2*A*. It may be that this is only slightly more likely than many other different configurations.

In the conventional striped state shown in Fig. 2 *C* and *D*, pairs of holes appear as the most probable state, but the state has only short-ranged pairing correlations and the small hole probability between the stripes suggests that the binding of the pairs to the stripes is suppressing superconductivity. In the W3 striped state shown in Fig. 2 *E* and *F*, the most probable state has the holes at their maximum separation within the stripes, with domain walls visible in the vertical direction across the holes, instead of the horizontal. This configuration is consistent with the idea that the stripes here imitate the 1D $t - J$ chain (42) and that one can view the holes as holons living in a squeezed Heisenberg chain of spins.

Scans Varying Doping and t'

We now discuss the scan calculations that were used in constructing the phase diagram. As shown in Fig. 3, in one set of scans, t' was fixed and the doping x was slowly varied along the length of the cylinder while in another set x was fixed and t' was varied. A linear variation of the chemical potential with the length l_x down the cylinder gave an essentially linear increase of the doping x. A similar application of a gradient in the chemical potential has also been utilized in cold-atom experiments (51). However, for the $t' = 0.2$ scan, it was necessary to vary the chemical potential slowly in the low-doping region where AFM, *d*-wave, and $\pi - p$-wave triplet pairing appeared. In the t'-varying case, the chemical potential also needed to be adjusted to keep the doping approximately constant across the system.[*]

A key feature of the scan calculations is to reduce the problem of metastable states. For fixed parameters (i.e., a non-

scan calculation) one may happen to be near a phase boundary, and determining which side one is on may involve small energy differences. In contrast, using a scan one is likely to pass through the phase boundaries, and the system will automatically adjust the location of the boundaries to account for the energies. The calculations are stabilized by the parts of the cylinder where the system is well within one phase or another.

In nonscan calculations where one is looking for a particular order, it is common to "pin the edges" with a corresponding field applied to the edge sites. This is not so clear-cut a procedure for a scan going through different phases, but, in fact, often in a DMRG calculation pinning fields are not necessary. Instead, DMRG can self-pin in a large 2D system. This aspect of DMRG calculations is well known among DMRG experts, but less so by others, so we give a detailed explanation of this effect in *SI Appendix*, section I. The gist is that DMRG tends to break a continuous symmetry and develop an order parameter just as a real experimental sample does. The broken symmetry goes away in the limit of large bond dimension, but for a range of moderate bond dimensions the system develops an order parameter similar in magnitude to that of the 2D thermodynamic limit. The required bond dimension to eliminate the broken symmetry increases rapidly with system size. Attempts to converge beyond this broken-symmetry plateau can be counterproductive, since in the symmetric phase the order can be seen only through correlation functions, and one can miss unexpected orders. In addition, correlation functions are inherently much less accurate than local measurements (52). In our scans, we use this effect to our advantage: In systems where there does appear to be robust *d*-wave SC, we do not pin it with an external field but rather we allow the system to self-pin. In systems where *d*-wave SC is suppressed, we apply a weak global pairing field. In this case, we may get some false positive signals of SC, but its absence is a clear sign that a superconducting state is not a low-energy state. In some cases we also apply a magnetic pinning field on one or both edges to reduce edge effects (53). It should be pointed out that such fields have almost no effect on the magnetic order in the bulk, which appear as long as we are in the "broken-symmetry plateau."

Fig. 3 shows an x-varying scan with a fixed $t' = 0.2$ corresponding to electron-doped cuprates. In the underdoped region we find coexisting uniform AFM, strong *d*-wave singlet pairing, and (π, π) *p*-wave triplet pairing (detailed discussion in *Electron Low-Doped Phase with Coexisting Uniform AFM, d-Wave Singlet, and (π, π) p-Wave Triplet Pairing*). As one increases doping away from half-filling, the pairing increases rapidly and $|\langle S_z \rangle|$ decreases slowly. When the doping is further increased beyond $x \sim 0.14$, conventional-looking stripes emerge. The transition to

---

[*]The chemical potential is of form $\mu(l_x) = \mu_0 + a\sqrt{1 + (b|2l_x - L_x|/L_x)^2}$ with a and b to be adjusted and different for the left and the right half. This form of chemical potential varies slower and connects smoothly in the middle.
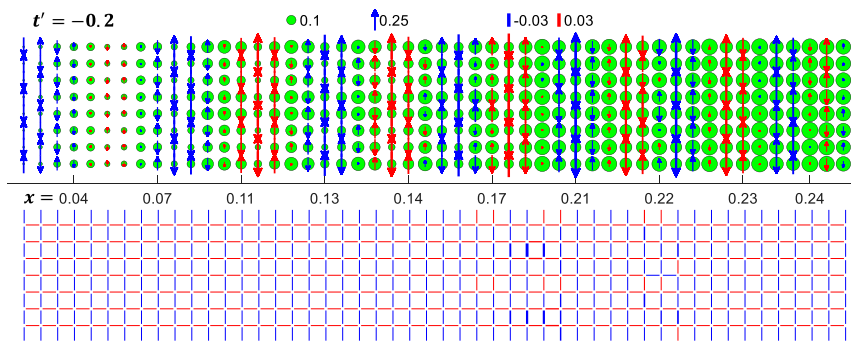
4 of 11 | **PNAS**
https://doi.org/10.1073/pnas.2109978118

Jiang et al.
Ground-state phase diagram of the t-t'-J model

Fig. 4. A doping-varying scan on a 50 × 8 cylinder with $t' = -0.2$, appropriate for hole-doped cuprates. A staggered magnetic pinning field of 0.03 is applied on the left edge. A global d-wave pairfield of 0.005 is applied to measure the pairing response. The system exhibits stripes across the whole doping range shown here with minimal pairing response to the applied pairing field.

stripes is rather sharp. The stripes still have robust pairing, but the magnitude of the order parameter is reduced. The point of optimal doping, where pairing is maximum, is near $x = 0.14$, in the uniform phase. Within the striped phase, pairing decreases with higher doping. It eventually disappears in a smooth way near $x \sim 0.25$ to 0.3.

Fig. 4 shows a similar x-varying scan but with $t' = -0.2$, corresponding to hole-doped cuprates. Other than a small region showing signs of the W3 striped phase around $x \sim 0.06$, the whole scan shows conventional stripes. As one increases doping, the magnitude of the density oscillations first increases until around $x = 0.2$ and then decreases. Pairing is almost completely suppressed despite a global d-wave pairfield of 0.005. Pairing remains weak even if the pairfield is made rather strong, say, 0.03. In terms of the pairing response and the applicability of the t-t'-J model to the cuprates, Figs. 3 and 4 indicate a clear contradiction: Pairing is much stronger in the hole-doped cuprates than we find in the t-t'-J model.

Fig. 5 shows an x-varying scan with $t' = 0$. While this case does not directly map to the cuprates, it has been studied often because of its simplicity. We find a hole density and spin pattern similar to the $t' = -0.2$ scan. Around $x \sim 0.07$ there are again some signs of a W3 striped phase, but separate calculations with fixed doping find this W3 stripe is metastable and higher in energy [$o(0.001t)$ per site] than the conventional striped phase at $t' = 0$. Despite a similar striped structure, the pairing response with $t' = 0$ is much stronger than at $t' = -0.2$. Under a global d-wave pairfield of 0.005, the pairing peaks around $x = 0.15$ with a value $\langle \Delta^\dagger + \Delta \rangle \sim 0.06$. If the pairfield is turned off, pairing decays slowly. We find that at $t' = 0$, the paired state is not the ground state when comparing its energy with the non-

paired state. In the global phase diagram, the boundary line where pairing appears is at slightly positive t'. This closeness of the boundary helps explain why in previous studies at $t' = 0$, it has been very difficult to determine whether the ground state is superconducting.

We now show another three scans where we keep x approximately constant and vary t' from 0.3 to -0.3. Fig. 6 shows a low-doping case, $x \sim 0.09$. The contrast between positive and negative t' is striking. For $t' > 0$ we find the AFM-$d/\pi p$ phase with uniform AFM and strong pairing. For $t' < 0$ we find conventional stripes and a rapid and strong suppression of the pairing response.

Fig. 7 shows a medium-doping $x \sim 0.13$. Here the boundary of uniform density versus stripe order has shifted to $t' \sim 0.1$. The striped state for $t' > 0$ has pairing, although it is weaker than in the AFM-$d/\pi p$ phase.

Fig. 8 shows a high-doping case with $x \sim 0.19$. In this case there are stripes for the whole range of t'. However, pairing order is present only for $t' \gtrsim 0.1$.

Electron Low-Doped Phase with Coexisting Uniform AFM, d-Wave Singlet, and (π, π) p-Wave Triplet Pairing

We now consider the individual phases in detail, starting with the phase with three order parameters at low doping and $t' > 0$. This region corresponds to electron-doped cuprates. There are two dominant orders: uniform AFM and a strong d-wave singlet pairing. As a result of these two orders there is also a (π, π) p-wave triplet pairing (AFM-$d/\pi p$) and it exists in a broad region defined roughly by $t' > 0$ and $x < 0.14$. Details of this phase for a nonscan calculation at $x = 0.12$ and $t' = 0.2$ are shown in Fig. 9. In Fig. 9 A and B we show the doping, spin, and singlet
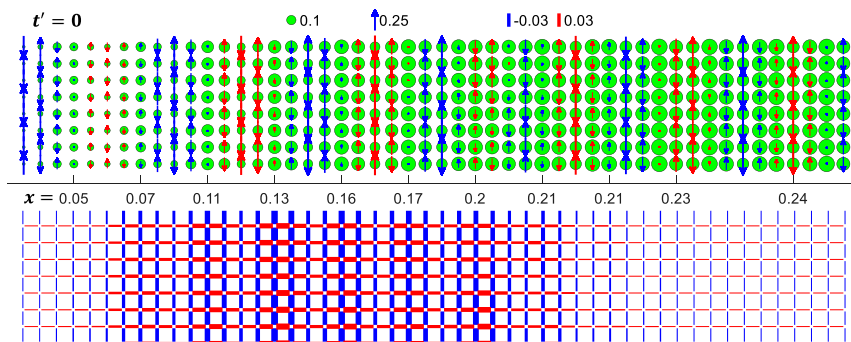

Fig. 5. A doping-varying scan on a 50 × 8 cylinder with $t' = 0$. A staggered magnetic pinning field of 0.05 is applied on both edges. A global d-wave pairfield of 0.005 is applied to measure the pairing response. The system is striped and pairing response peaks near $x = 0.15$, but in nonscan calculation without applied field the system shows no local pairing and the pair–pair correlations die rapidly with separation.
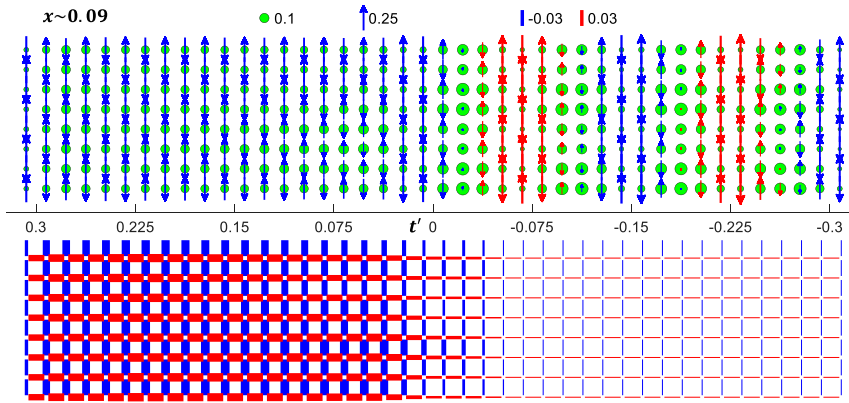
Jiang et al.
Ground-state phase diagram of the t-t'-J model

PNAS | 5 of 11
https://doi.org/10.1073/pnas.2109978118

Fig. 6. A t'-varying scan on a 42×8 cylinder with doping $x \sim 0.09$. A staggered magnetic pinning field of 0.03 is applied on both edges. No pairfield is applied. For $t' > 0$ we see the AFM-$d/\pi p$ phase, while in the region with negative t' we find a conventional stripe phase and pairing is suppressed.

pairing expectation values. All these quantities are uniform across the system. No applied pairing field was used. The presence of nonzero pairing order helps the density become more uniform, counteracting any oscillations due to the open boundaries. The magnitude of the pairing order is $\langle \Delta_s^\dagger + \Delta_s \rangle = 0.081$, and the difference in sign between vertical and horizontal bonds signifies d-wave order. We judge the size of the order parameter to be quite large; in particular, if one does apply a pairing field, one cannot readily make it much larger. Also, the simulations are clear and unambiguous; there do not appear to be any other competing states. Starting from a nonpairing initial product state, the system spontaneously breaks particle-conservation symmetry and produces the pairing order. As mentioned before, *SI Appendix*, section I has a detailed discussion for spontaneously broken symmetry in DMRG.

As shown in Fig. 9C we also observe a smaller (π, π) p-wave triplet pairing in addition to the strong d-wave singlet pairing. It is uniform in amplitude and has (π, π) $p_x - p_y$ form:

$$\langle \Delta_t (l_x, l_y) \rangle = e^{i\pi(l_x + l_y)} [\langle \Delta_t (l_x, l_y, x) \rangle - \langle \Delta_t (l_x, l_y, y) \rangle] \quad [\textbf{3}]$$

with $\Delta_t(l_x, l_y, x/y)$ being a triplet pairing on a horizontal/vertical link with left/lower site (l_x, l_y). The overall phase of triplet pairing is determined by the overall phase of the AFM order and d-wave pairing. This triplet order is a consequence of the other two orders, not a competing order. As mentioned before, the existence of AFM order breaks SU(2) spin symmetry, so that singlet and triplet pairings are no longer distinct, making the

d-wave pairing have a triplet component. The nonzero wavevector reflects the wavevector of the AFM order. The magnitude of the triplet pairing is roughly proportional to that of the singlet pairing, $\langle \Delta_t \rangle / \langle \Delta_s \rangle \approx 0.4$, if no magnetic field is applied, and this ratio is mostly t' independent.

To further study the interplay of AFM, singlet, and triplet pairing, we applied a global staggered magnetic field to the system, which directly enhances the AFM order. Fig. 9D shows that under this field, both magnetization and triplet pairing are enhanced while singlet pairing is mostly unchanged. It is interesting that there is no competition between strong AFM order and d-wave pairing; they happily coexist, but as a consequence of increased AFM order the triplet order gets larger. Defining $A(x)$ through the following relation between these three quantities,

$$\langle \Delta_t \rangle = A(x) \langle \Delta_s \rangle \langle S_z \rangle, \quad [\textbf{4}]$$

we find that $A(x)$ varies slowly with doping (2.3 for $x = 0.12$, 2.0 for $x = 0.065$). We further verify that this relation holds when a global d-wave singlet pairfield is applied. This relation is qualitatively consistent with several studies where there is coexistence of AFM, d-wave singlet pairing, and (π, π) p-wave triplet pairing (37, 38, 44). This further implies that this $(\pi, \pi) p$-wave triplet pairing is purely parasitic and relies on the existence of both AFM and d-wave singlet pairing.

Fig. 7. A t'-varying scan on a 40×8 cylinder with doping $x \sim 0.13$. No pairfield is applied. A staggered magnetic pinning field of 0.03 is applied on both edges. For $t' > 0$ we see the AFM-$d/\pi p$ phase, which becomes striped for smaller t'. In the negative t' region the stripes continue but without pairing.
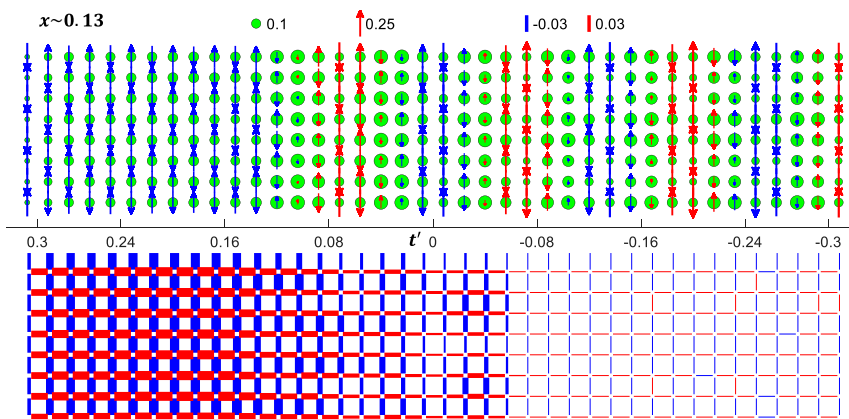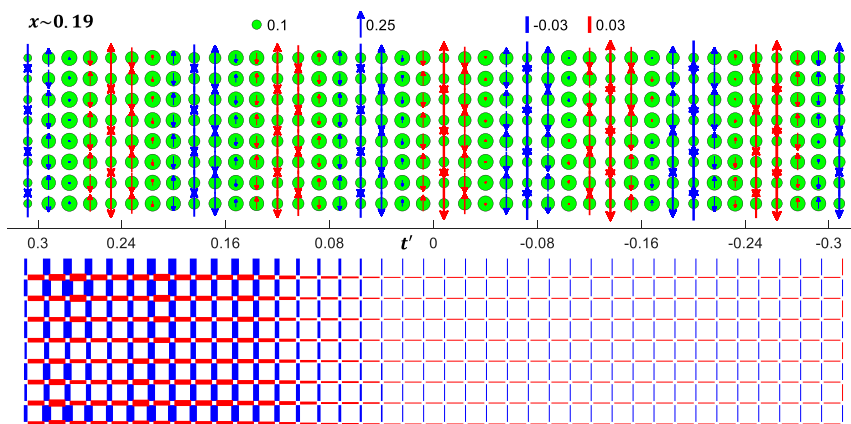
Fig. 8. A t'-varying scan on a 40×8 cylinder with doping $x \sim 0.19$. No pairfield is applied. A staggered magnetic pinning field of 0.03 is applied on both edges. There are stripes across the whole system, but pairing only for larger positive t'.

Higher Electron Doping Phase: Stripes with d-Wave Singlet and Striped p-Wave Pairing

In the electron-overdoped, $t' > 0$ region of the phase diagram we observe a striped phase with roughly uniform d-wave singlet pairing and modulated p-wave triplet pairing. In Fig. 10 A–C we show local expectation values for a point in this phase at $x = 0.20$ and $t' = 0.2$. The striped phase looks like stripes at $t' < 0$ if one looks only at the charge and spin. Unlike that case, here we have clear d-wave pairing, although not as strong as at lower doping. In this case, starting in a product state, the system can get stuck in an unpaired state, but applying a pairfield for a few sweeps allows it to go to the lower-energy [by about $o(0.001t)$ per site] paired state with a singlet pairing order $\langle \Delta_s^\dagger + \Delta_s \rangle = 0.044$. (In a width-6 system, the unpaired state is not metastable; starting from a product state, the DMRG sweeps readily find the paired state. More comparisons with width-6 systems are made in *SI Appendix*, section III.) The pairing is only slightly larger on the domain walls compared to the region in-between them, as shown in Fig. 10D.

Because there are local AFM regions between the stripes, one would expect also a triplet pairing component to appear. Fig. 10C shows the p-wave triplet pairing for this system. Interestingly, the p-wave triplet pairing $\langle \Delta_t \rangle$ that is modulated by stripes shows a wave-like amplitude as one can see more clearly in Fig. 10D. In contrast to the Δ_s that is only slightly bigger at the domain walls, the Δ_t order has nodes at the domain walls, reflecting its parasitic dependency on the AFM order.

Conventional Stripe Phase and Low-Doped W3 Stripe Phase

While the striped phase described in the previous section has a ground state with pairing, in a broader parameter region that includes the whole $t' < 0$ part except for extreme low doping, stripes still form but the ground state has no pairing. This phase is the conventional striped phase.

The hole and spin pattern of conventional stripes without pairing is very similar to that of stripes with pairing. One small difference, which one can see by comparing Figs. 3 and 4, is that the stripes at $t' = 0.2$ are homogeneous in hole density and spin
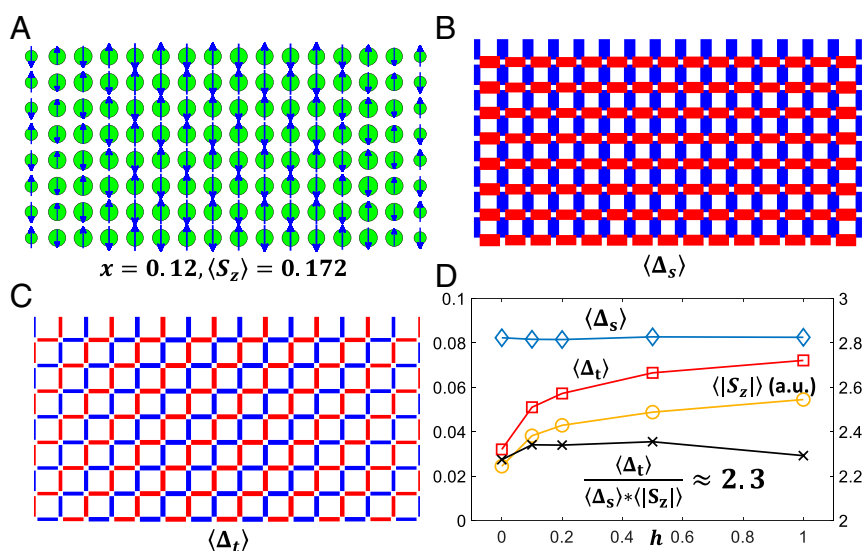

Fig. 9. The AFM-$d/\pi p$ phase at fixed $t' = 0.2$ and $x = 0.12$. A and B show spin, charge, and d-wave singlet pairing as in previous plots. In C, we show triplet link pairing, where we find (π, π) p-wave order. For D, we plot singlet and triplet pairing, as well as the spin expectation value (left-axis scale), for systems that have had a global staggered magnetic field h applied; each value of h is a different simulation. The singlet pairing is nearly independent of h while the triplet pairing and magnetization both increase with h, but the indicated ratio (black crosses, right axis) is nearly constant.

Jiang et al.
Ground-state phase diagram of the t-t'-J model

PNAS | 7 of 11
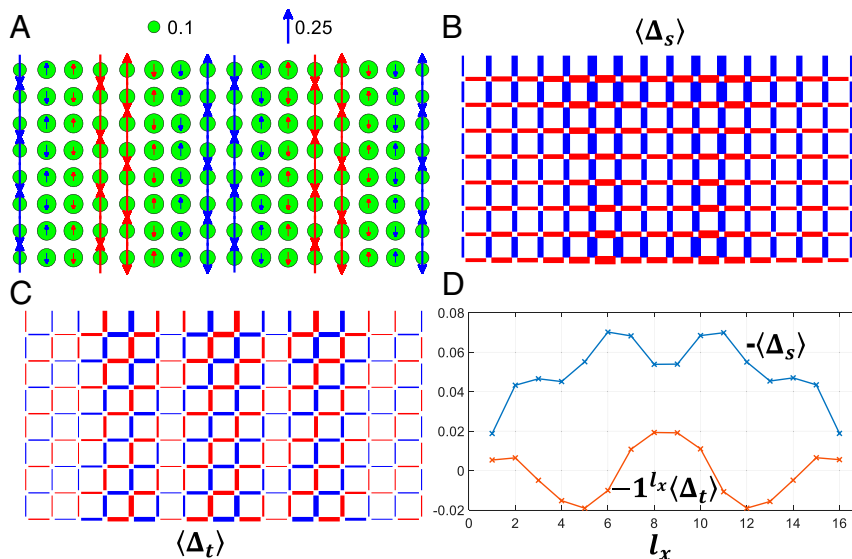https://doi.org/10.1073/pnas.2109978118

Fig. 10. Higher-doped positive t' phase with stripes and pairing. The doping is $x = 0.20$ and $t' = 0.2$. A–C are as in Fig. 9. In C, we see that the p pairing is modulated by the domain walls in the antiferromagnetism. This is apparent in D, which shows the singlet pairing and the triplet pairing multiplied by -1^{l_x} versus l_x. The singlet pairing has small modulations with peaks at the stripes, while the triplet pairing oscillates with nodes at the stripes.

along the stripes, while at $t' = -0.2$ there is a small modulation along each stripe. The difference in pairing is much more significant: The conventional striped state is nonsuperconducting. A state with pairing is nearby for t' near 0, and it can be seen as a metastable state in DMRG, but its energy rises as t' is made more negative and it is no longer metastable. For $t' = -0.2$, even a strong global pairfield triggers only a weak pairing response and the pair–pair correlation function shows exponential decay.

The W3 striped phase is distinct from the conventional striped phase, although both occur for $t' < 0$. Fig. 11 shows nonscan results for the W3 phase, at a doping of 0.08, at $t' = -0.2$. The key to understanding the W3 phase is a Heisenberg two-leg ladder. A two-leg ladder has a spin gap of about $J/2$, and

we can think of this gap as not just the raising of excited-state energies, but also the lowering of the ground-state energy, making width-2 undoped ladder regions favored. The two-leg Heisenberg spin ladder has short-range spin correlations, with a correlation length of about 3.19 (41). This is in contrast to, say, a three-leg ladder that is gapless with power-law spin correlations. We do not find a W4 phase similar to the W3 phase but with three-leg ladders; the two-leg ladder W3 configuration is the only such phase found. The stripes themselves resemble t-J chains, with one hole per about four lattice spacings; holes are unbound, and there is strong hopping along the chain. There is also transverse hopping onto the ladders but this seems predominantly a single hop away from the chains. In the spin-squeezed picture of the t-J chain (42), the holes act as mobile
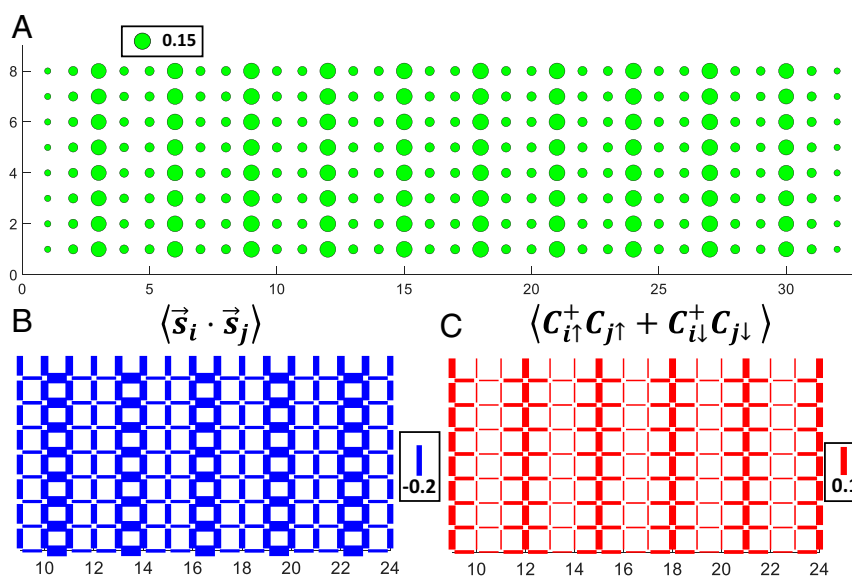

Fig. 11. W3 striped phase on a 32 × 8 cylinder at $x = 0.08$, $t' = -0.2$. In A only the local doping is shown; the local spin measurements are zero. The stripes are strongly associated with single columns. In B we show the nearest-neighbor spin–spin correlations, which are much stronger in the undoped width-2 "ladders." Longer-distance spin–spin correlations are measured to decay rapidly. In C we show the link hopping, which is very strong along the stripes but also exhibits limited hops onto the ladders. The results together suggest significant decoupling between the chains and ladders.
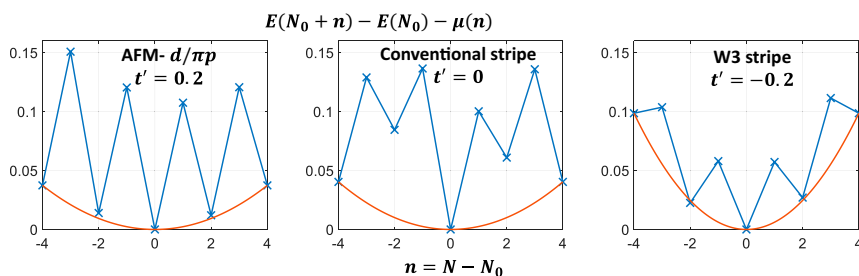
8 of 11 | PNAS
https://doi.org/10.1073/pnas.2109978118

Jiang et al.
Ground-state phase diagram of the t-t'-J model

$$E(N_0 + n) - E(N_0) - \mu(n)$$

Fig. 12. Energy versus number of particles, from which one can read off various gaps. The overall curvature is the result of using a finite-length cylinder (32×6); the orange curve shows a quadratic fit to the points touching it. The chemical potential has been set to make the slope at the midpoint zero. (*Left*) AFM-$d/\pi p$ phase with $t' = 0.2$ at $x \sim 0.08$. (*Center*) Conventional striped phase with $t' = 0$ at $x \sim 0.08$. (*Right*) W3 striped phase with $t' = -0.2$ at $x \sim 0.07$. Here the W3 stripe runs horizontally on width 6, displayed in *SI Appendix*, Fig. S5B.

domain walls in a Heisenberg chain; thus, for example, instantaneous singlet spin correlations are present across each hole. There is no attraction between holes. All these features seem to also describe the stripes in the W3 phase. The W3 phase seems even farther from superconducting than the conventional striped phase: There is no sign of paired holes (Fig. 2F).

In the W3 phase the spin correlations are short ranged in both directions. The low doping of each stripe and the weak transverse hopping make them unable to create π-phase shifts in the local AFM correlations. There are negligible spin correlations between the ladders. Within the ladders, vertical-separation spin–spin correlations are also short ranged, with a much more rapid decay compared to the conventional striped phase.

The W3 stripe shown in Fig. 11 is at its ideal filling for a width-8 cylinder: two holes per three columns or a doping of $x = \frac{2}{24} = 0.0833$. If we decrease the doping, the phase does not change in a smooth way on width 8. Two holes per stripe and two-leg-ladder undoped regions are both favored in a quantized way. Decreasing the doping on width 8 causes defects (*SI Appendix*, Fig. S6): limited regions that have wider spacing so that most of the cylinder can maintain a spacing of 3 between stripes. If the two-leg Heisenberg ladder picture is correct for the W3 phase, then the spacing of 3 would hold on any width cylinder. However, there is nothing in this picture that says the spacing of holes along a stripe must be exactly 4. We do not expect an odd number of holes per stripe, as that would require a spin excitation. However, one might have different spacings on a much wider cylinder: For example, one might find four-hole stripes not just on a width-16 cylinder, but also, say, on widths 14 and 18.

Another system where we can see the W3 phase is a width-6 cylinder, where the stripes run along the length of the cylinder. This is shown in *SI Appendix*, Fig. S5B. In this case two stripes and two ladders just fit. In the width-6 cylinder, we do find the spacing of holes on each stripe can be varied away from 4 slightly by adjusting the doping, consistent with the discussion above for wide cylinders.

Energy Gaps

We can get further insight into the nature of the phases by studying their energy gaps associated with adding or removing particles. A generic formula for this sort of energy gap is

$$\Delta E_n = [E(N_0 + n) + E(N_0 - n) - 2E(N_0)]/2, \qquad [5]$$

for adding or removing n particles at a time, where $E(N)$ is the ground-state energy with N particles. This formula exhibits finite-size effects due to the finite size of the system. The finite length manifests as an overall curvature of $E(N)$, which can be viewed as a shift in the chemical potential with N. In an infinite system, the chemical potential would not shift when adding a finite number of particles.

Rather than extrapolations in system size, we find it more convenient to plot $E(N)$ directly and fit the lower envelope of points to a quadratic function. This is shown in Fig. 12. The gaps are then measured by how many points rise above the quadratic fit. These calculations were done on a width-6 system for higher accuracy. For the W3 stripe calculations on width 6, two stripes run in the horizontal direction, as shown in *SI Appendix*, Fig. S5B. Changing the number of particles changes the filling of these two stripes.

In the AFM-$d/\pi p$ phase, we see that an odd number of particles is higher in energy. This is because in this superconducting phase, an odd-N system has an extra quasiparticle, and we interpret the associated gap as the superconducting gap. Here, this is about 0.12. There is no sign of gaps associated with higher numbers of particles. In contrast, in the conventional stripe
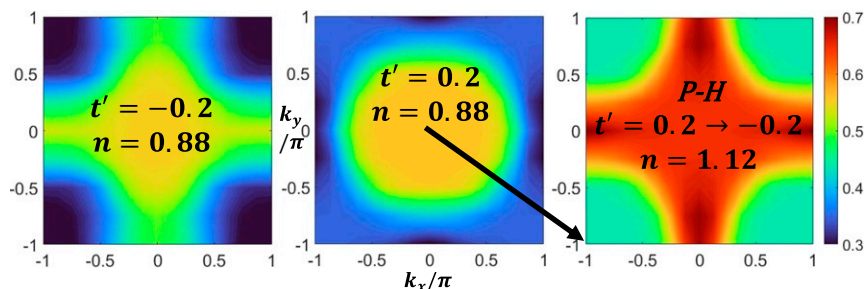

Fig. 13. Momentum space occupancy $n(\vec{k})$ for a single spin in the width-8 cylinder. *Left* shows $n(\vec{k})$ for the fermions in the t-t'-J model with $t' = -0.2$ and $n = 0.88$ fermions per site. This corresponds to the momentum distribution for the electrons in a hole-doped system. *Center* shows the momentum distribution of the fermions in the t-t'-J model with $n = 0.88$ fermions per site and $t' = 0.2$. Under a particle–hole transformation, which includes a (π, π) shift of the origin, one obtains the plot on *Right*. Here $n(\vec{k})$ represents the momentum occupation of the electrons for an electron-doped system with $t' = -0.2$ and $n = 1.12$ electrons per site.

Jiang et al.
Ground-state phase diagram of the t-t'-J model

PNAS | 9 of 11
https://doi.org/10.1073/pnas.2109978118

phase, we see two gaps involved. Systems with odd N exhibit the highest energies, corresponding to broken pairs. However, we also see that in the even-N sector, multiples of four are lower in energy than nonmultiples of four. This is because the stripes in this system have four holes, composed of two pairs, which are bound. A nonmultiple of four must have an isolated pair (*SI Appendix*, Fig. S5A), with an energy higher by about 0.05.

In Fig. 12, *Right* showing a W3 striped phase, we see a smaller single-particle gap compared to the previous two cases. This state is unpaired but the energy is still sensitive to having half-integer total spin. One would expect an extra fermion mainly living in a stripe, since a t-J chain is gapless but a Heisenberg ladder has a large spin gap. It is not clear whether the finite gap seen is a consequence of the finite length, the even circumference of the cylinder, or some other effect.

Comparison to Cuprates

To test the applicability of our model to cuprates, we first look at the momentum distribution function $n(\vec{k})$ by measuring the single-particle Green's function in real space and Fourier transforming it. The results are shown in in Fig. 13. Both cases are for a fermion doping of $x \approx 0.125$ of the t-t'-J model. In Fig. 13, *Left* with $t' = -0.2$, x represents the hole doping and $n(\vec{k})$ is the momentum occupation of the electrons for a hole-doped system with $n = 1 - x \sim 0.875$ electrons per site. This Fermi surface is similar to what is seen in the hole-doped cuprates. In Fig. 13, *Center* with $t' = 0.2$, the fermions occupy a circular region centered at the origin. *Right*, under a particle–hole transformation, $\vec{k}$ is shifted by (π, π) and these fermions represent holes in a region centered about (π, π). In this case, the system is electron doped with $n = 1 + x \sim 1.125$ electrons per site and has a Fermi surface that is similar to what is seen in the electron-doped cuprates.

If we collect the AFM, charge-ordered (CO), and SC pairing from the various scans with $t' = 0.2$ and $t' = -0.2$, we can construct a zero-temperature order parameter diagram as shown in Fig. 14, *Lower*. This can be compared to the nominal cuprates phase diagram in Fig. 14, *Upper* taken from ref. 54, where here the vertical axis is temperature. We see several similarities: a much broader AFM dome on the electron-doped side than on the hole-doped side and a charge-ordered region at intermediate doping on both sides. However, contrary to the cuprate phase diagram, the SC pairing is significantly suppressed on the hole-doped side with $t' = -0.2$, whereas in the hole-doped cuprates there is a broad SC dome. Moreover, on the electron-doped side with $t' = 0.2$, we find that the t-t'-J model exhibits a broad range of doping over which there is coexisting AFM, d-wave SC, and π-triplet–p-wave SC order, contrary to what is observed in the cuprate phase diagram. In this paper we have set $J = 0.4$. However, for $J = 1/3$ we have checked four key points in the phase diagram and find the same four phases: the AFM-$d/\pi p$ phase at low electron doping ($t' = 0.2$, $x = 0.0625$), the stripes with pairing at high electron doping ($t' = 0.2$, $x = 0.19$), the W3 stripe phase at low hole doping ($t' = -0.2$, $x = 0.0833$), and the conventional stripe without pairing phase at high hole doping ($t' = -0.2$, $x = 0.19$).

Thus, we conclude that one must go beyond the t-t'-J model to understand superconductivity in the cuprates. This immediately suggests an important question: Would a Hubbard model with t' do better? In renormalizing the two particle states to go from the Hubbard to the t-t'-J model, there are terms that are of the same order as J that are omitted (55). It could be that these terms are important for representing the physics of the cuprates. Alternatively, it may be that other interactions are needed to represent superconductivity properly.
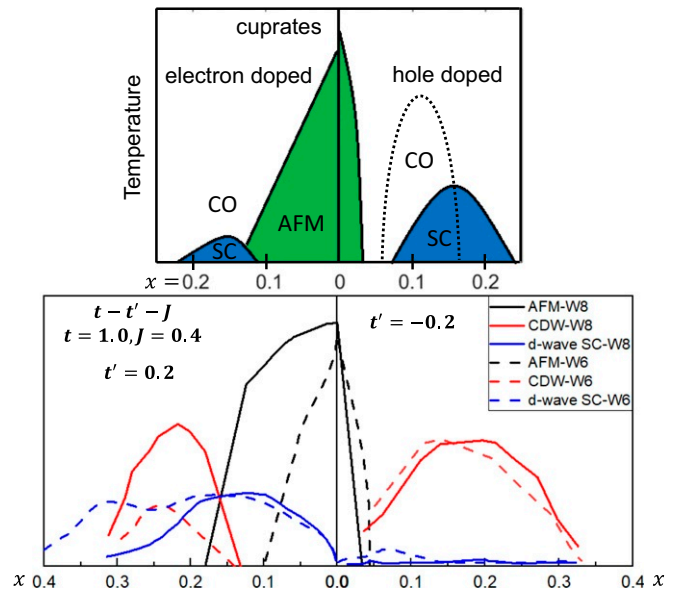

Fig. 14. (*Upper*) Experimental phase diagram of a typical cuprate superconductor, following ref. 55, with AFM, CO, and SC phases. The vertical axis is temperature and horizontal axis indicates electron doping (*Left* side) and hole doping (*Right* side). (*Lower*) Antiferromagnetic, superconducting, and charge-density wave order parameters at zero temperature in the t-t'-J model from DMRG calculations. Solid lines are for width-8 (W8) cylinders and dashed lines are for width-6 (W6) cylinders.

Summary

We have carried out large-scale ground-state DMRG calculations on t-t'-J cylinders with widths 6 and 8, which approximate the behavior of 2D systems. We have established an approximate phase diagram for this model.

On the positive t' side, which corresponds to electron-doped cuprates, at low doping we find an AFM-$d/\pi p$ phase with coexisting uniform AFM and strong d-wave singlet pairing. As a result of these two orders, there also exists (π, π), p-wave triplet pairing. Pairing in this electron low-doped region is strong and unambiguous. At higher doping there is a striped phase with relatively weaker d-wave singlet pairing, as well as triplet pairing with an amplitude modulated by the stripes.

On the negative t' side, which corresponds to hole-doped cuprates, there is a broad striped phase. States with pairing go from being metastable and only slightly higher in energy near $t' = 0$ to significantly suppressed with $t' = -0.2$. At low doping, near $x = 0.08$, we find an unconventional width-3 stripe phase that has chains of unpaired holes separated by two-leg spin ladders. The hole chains behave like 1D t-J chains while spins on two-leg ladders mimic the short-ranged spin correlations seen in two-leg Heisenberg ladders. For $t' < 0$, AFM order exists only for a very narrow doping range near half-filling.

Despite the fact that this t-t'-J model manages to capture several aspects of the electron- and hole-doped cuprates, including the broad AFM dome on the electron side and a much more narrow one on the hole side, as well as charge order on both sides, the superconducting properties exhibit significant discrepancies with respect to the cuprates. The hole-doped cuprates exhibit strong superconductivity while the corresponding region of the model does not. In contrast, for the electron-doped region of the model we find strong superconductivity over a broader doping range than in the cuprates, and for a substantial range of doping this pairing coexists with AFM and triplet p-wave superconductivity.

10 of 11 | PNAS
https://doi.org/10.1073/pnas.2109978118

Jiang et al.
Ground-state phase diagram of the t-t'-J model

Materials and Methods

We use finite-system DMRG using the ITensor library (39).

Data Availability. Data generated by DMRG calculation are explicitly stated or deposited in Figshare, dx.doi.org/10.608c4/m9.figshare.14687631 (56).

Note. As this paper was being finished, S. Gong, W. Zhu, and D. N. Sheng posted a preprint where DMRG was used to study superconducting, magnetic, and charge correlations on width-4 and -6 t-t'-J cylinders (57). Their main conclusion was that for $t' > 0$ there appears to be robust d-wave superconductivity. Although their phase diagram differs in several respects from ours, we believe their correlation functions are quite consistent with ours. In particular, they find AFM correlations in the AFM-$d/\pi p$

region of the phase diagram that decay exponentially but with a rapidly increasing correlation length going from width 4 to 6. In our results, we also find the AFM correlations have a similar decay on width 6, but by width 8 the correlations always extend beyond the length of the systems we study, manifesting as long-range order with a broken-symmetry ground state. More detailed discussion about magnetic order and correlation function in the AFM-$d/\pi p$ phase can be found in *SI Appendix, section II*.

1. B. X. Zheng *et al.*, Stripe order in the underdoped region of the two-dimensional Hubbard model. *Science* **358**, 1155–1160 (2017).
2. M. Qin *et al.*, Absence of superconductivity in the pure two-dimensional Hubbard model. *Phys. Rev. X* **10**, 031016 (2020).
3. D. P. Arovas, E. Berg, S. Kivelson, S. Raghu, The Hubbard model. arXiv [Preprint] (2021). https://arxiv.org/abs/2103.12097 (Accessed 22 March 2021).
4. M. Qin, T. Schafer, S. Andergassen, P. Corboz, E. Gull, The Hubbard model: A computational perspective. arXiv [Preprint] (2021). https://arxiv.org/abs/2104.00064 (Accessed 31 March 2021).
5. H. C. Jiang, T. P. Devereaux, Superconductivity in the doped Hubbard model and its interplay with next-nearest hopping t'. *Science* **365**, 1424–1428 (2019).
6. Y. F. Jiang, J. Zaanen, T. P. Devereaux, H. C. Jiang, Ground state phase diagram of the doped Hubbard model on the four-leg cylinder. *Phys. Rev. Res.* **2**, 033073 (2020).
7. E. W. Huang, C. B. Mendl, H. C. Jiang, B. Moritz, T. P. Devereaux, Stripe order from the perspective of the Hubbard model. *Quantum Materials* **3**, 1–6 (2018).
8. J. F. Dodaro, H. C. Jiang, S. A. Kivelson, Intertwined order in a frustrated four-leg t-J cylinder. *Phys. Rev. B* **95**, 155116 (2017).
9. C. M. Chung, M. Qin, S. Zhang, U. Schollwöck, S. R. White, Plaquette versus ordinary -wave pairing in the t'-Hubbard model on a width-4 cylinder. *Phys. Rev. B* **102**, 041106 (2020).
10. H. C. Jiang, Z. Y. Weng, S. A. Kivelson, Superconductivity in the doped t-J model: Results for four-leg cylinders. *Phys. Rev. B* **98**, 140505 (2018).
11. K. Ido, T. Ohgoe, M. Imada, Competition among various charge-inhomogeneous states and d-wave superconducting state in Hubbard models on square lattices. *Phys. Rev. B* **97**, 045138 (2018).
12. L. F. Tocchio, F. Becca, S. Sorella, Hidden Mott transition and large-u superconductivity in the two-dimensional Hubbard model. *Phys. Rev. B* **94**, 195126 (2016).
13. P. Corboz, T. M. Rice, M. Troyer, Competing states in the t-J model: Uniform D-wave state versus stripe state. *Phys. Rev. Lett.* **113**, 046402 (2014).
14. P. Corboz, S. R. White, G. Vidal, M. Troyer, Stripes in the two-dimensional t-J model with infinite projected entangled-pair states. *Phys. Rev. B* **84**, 041108 (2011).
15. J. P. F. LeBlanc *et al.*, Solutions of the two-dimensional Hubbard model: Benchmarks and results from a wide range of numerical algorithms. *Phys. Rev. X* **5**, 041041 (2015).
16. S. R. White, D. J. Scalapino, Pairing on striped t-J lattices. *Phys. Rev. B* **79**, 220504 (2009).
17. B. Ponsioen, S. S. Chung, P. Corboz, Period 4 stripe in the extended two-dimensional Hubbard model. *Phys. Rev. B* **100**, 195141 (2019).
18. A. Himeda, T. Kato, M. Ogata, Stripe states with spatially oscillating d-wave superconductivity in the two-dimensional t-t'-J model. *Phys. Rev. Lett.* **88**, 117001 (2002).
19. X. Y. Xu, T. Grover, Competing nodal d-wave superconductivity and antiferromagnetism. *Phys. Rev. Lett.* **126**, 217002 (2020).
20. H. C. Jiang, S. A. Kivelson, High temperature superconductivity in a lightly doped quantum spin liquid, *Phys. Rev. Lett.* **127**, 097002 (2021).
21. T. Tohyama, M. Mori, S. Sota, Dynamical density matrix renormalization group study of spin and charge excitations in the four-leg t-t'-J ladder. *Phys. Rev. B* **97**, 235137 (2018).
22. J. Zaanen, O. Gunnarsson, Charged magnetic domain lines and the magnetism of high-Tc oxides. *Phys. Rev. B Condens. Matter* **40**, 7391–7394 (1989).
23. D. Poilblanc, T. M. Rice, Charged solitons in the Hartree-Fock approximation to the large-U Hubbard model. *Phys. Rev. B Condens. Matter* **39**, 9749–9752 (1989).
24. K. Machida, Magnetism in La$_2$CuO$_4$ based compounds. *Physica C* **158**, 192–196 (1989).
25. M. Kato, K. Machida, H. Nakanishi, M. Fujita, Soliton lattice modulation of incommensurate spin density wave in two dimensional Hubbard model-a mean field study. *J. Phys. Soc. Jpn.* **59**, 1047–1058 (1990).
26. S. R. White, Density matrix formulation for quantum renormalization groups. *Phys. Rev. Lett.* **69**, 2863–2866 (1992).
27. S. R. White, Density-matrix algorithms for quantum renormalization groups. *Phys. Rev. B Condens. Matter* **48**, 10345–10356 (1993).
28. S. R. White, D. J. Scalapino, Density matrix renormalization group study of the striped phase in the 2d t-J model. *Phys. Rev. Lett.* **80**, 1272–1275 (1998).
29. F. Becca, L. Capriotti, S. Sorella, Stripes and spin incommensurabilities are favored by lattice anisotropies. *Phys. Rev. Lett.* **87**, 167005 (2001).
30. S. Sorella *et al.*, Superconductivity in the two-dimensional t-J model. *Phys. Rev. Lett.* **88**, 117002 (2002).
31. C. P. Chou, T. K. Lee, Mechanism of formation of half-doped stripes in underdoped cuprates. *Phys. Rev. B Condens. Matter Mater. Phys.* **81**, 060503 (2010).
32. L. F. Tocchio, A. Montorsi, F. Becca, Metallic and insulating stripes and their relation with superconductivity in the doped Hubbard model. *SciPost Phys.* **7**, 21 (2019).
33. S. R. White, D. J. Scalapino, Competition between stripes and pairing in a t-t'-J model. *Phys. Rev. B Condens. Matter Mater. Phys.* **60**, R753–R756 (1999).
34. G. Psaltakis, E. Fenton, Superconductivity and spin-density waves: Organic superconductors. *J. Phys. C Solid State Phys.* **16**, 3913 (1983).
35. S. C. Zhang, A unified theory based on SO(5) symmetry of superconductivity and antiferromagnetism. *Science* **275**, 1089–1096 (1997).
36. A. Aperis, G. Varelogiannis, P. Littlewood, B. Simons, Coexistence of spin density wave, d-wave singlet and staggered π-triplet superconductivity. *J. Phys. Condens. Matter* **20**, 434235 (2008).
37. W. Rowe, J. Knolle, I. Eremin, P. J. Hirschfeld, Spin excitations in layered antiferromagnetic metals and superconductors. *Phys. Rev. B* **86**, 134513 (2012).
38. D. E. Almeida, R. M. Fernandes, E. Miranda, Induced spin-triplet pairing in the coexistence state of antiferromagnetism and singlet superconductivity: Collective modes and microscopic properties. *Phys. Rev. B* **96**, 014514 (2017).
39. M. Fishman, S. R. White, E. M. Stoudenmire, The ITensor software library for tensor network calculations. arXiv [Preprint] (2020). https://arxiv.org/abs/2007.14822 (Accessed 28 July 2020).
40. D. J. Scalapino, The case for $d_{x^2-y^2}$ pairing in the cuprate superconductors. *Phys. Rep.* **250**, 329–365 (1995).
41. S. R. White, R. M. Noack, D. J. Scalapino, Resonating valence bond theory of coupled Heisenberg chains. *Phys. Rev. Lett.* **73**, 886–889 (1994).
42. T. Xiang, N. d'Ambrumenil, Charge-spin separation and the ground-state wave function of the one-dimensional t-J model. *Phys. Rev. B Condens. Matter* **45**, 8150–8153 (1992).
43. D. Sénéchal, P. L. Lavertu, M. A. Marois, A. M. S. Tremblay, Competition between antiferromagnetism and superconductivity in high-Tc cuprates. *Phys. Rev. Lett.* **94**, 156404 (2005).
44. A. Foley, S. Verret, A. M. S. Tremblay, D. Sénéchal, Coexistence of superconductivity and antiferromagnetism in the Hubbard model for cuprates. *Phys. Rev. B* **99**, 184510 (2019).
45. B. Kyung, Mean-field study of the interplay between antiferromagnetism and d-wave superconductivity. *Phys. Rev. B* **62**, 9083 (2000).
46. M. Kato, K. Machida, Superconductivity and spin-density waves: Application to heavy-fermion materials. *Phys. Rev. B Condens. Matter* **37**, 1510–1519 (1988).
47. K. Machida, K. Nokura, T. Matsubara, Theory of antiferromagnetic superconductors. *Phys. Rev. B Condens. Matter* **22**, 2307–2317 (1980).
48. M. Murakami, H. Fukuyama, Backward scattering and coexistent state in two-dimensional electron system. *J. Phys. Soc. Jpn.* **67**, 2784–2791 (1998).
49. E. Jeckelmann, D. J. Scalapino, S. R. White, Comparison of different ladder models. *Phys. Rev. B* **58**, 9492 (1998).
50. S. R. White, D. J. Scalapino, Hole and pair structures in the t-J model. *Phys. Rev. B* **55**, 6504 (1997).
51. S. Krinner, T. Esslinger, J. P. Brantut, Two-terminal transport measurements with cold atoms. *J. Phys. Condens. Matter* **29**, 343003 (2017).
52. S. R. White, A. L. Chernyshev, Neél order in square and triangular lattice Heisenberg models. *Phys. Rev. Lett.* **99**, 127004 (2007).
53. E. M. Stoudenmire, S. R. White, Studying two-dimensional systems with the density matrix renormalization group. *Annu. Rev. Condens. Matter Phys.* **3**, 111–128 (2012).
54. E. H. da Silva Neto *et al.*, Charge ordering in the electron-doped superconductor Nd$_{2-x}$Ce$_x$CuO$_4$. *Science* **347**, 282–285 (2015).
55. V. I. Belinicher, A. L. Chernyshev, V. A. Shubin, Generalized t-t'-J model: Parameters and single-particle spectrum for electrons and holes in copper oxides. *Phys. Rev. B Condens. Matter* **53**, 335–342 (1996).
56. S. Jiang, Data for figures. Figshare. https://doi.org/10.6084/m9.figshare.14687631. Deposited 27 May 2021.
57. S. Gong, W. Zhu, D. N. Sheng, Robust d-wave superconductivity in the square-lattice t-j model. *Phys. Rev. Lett.* **127**, 097003 (2021).

Jiang et al.
Ground-state phase diagram of the *t-t'-J* model

PNAS | 11 of 11
https://doi.org/10.1073/pnas.2109978118